



Contents lists available at ScienceDirect

Biomaterials

journal homepage: www.elsevier.com/locate/biomaterials

The use of hollow mesoporous silica nanospheres to encapsulate bortezomib and improve efficacy for non-small cell lung cancer therapy

Jia Shen^{a,b,c,1}, Guosheng Song^{d,1}, Man An^{a,c}, Xianqian Li^e, Ning Wu^e, Kangcheng Ruan^{a,c}, Junqing Hu^{d,**}, Ronggui Hu^{a,c,*}

^a State Key Laboratory of Molecular Biology, Institute of Biochemistry and Cell Biology, Shanghai Institutes for Biological Sciences, Chinese Academy of Sciences, 320 Yue-yang Road, Shanghai 200031, China

^b University of Chinese Academy of Sciences, Institute of Biochemistry and Cell Biology, Shanghai Institutes for Biological Sciences, Chinese Academy of Sciences, 320 Yue-yang Road, Shanghai 200031, China

^c Shanghai Key Laboratory of Molecular Andrology, Institute of Biochemistry and Cell Biology, Shanghai Institutes for Biological Sciences, Chinese Academy of Sciences, 320 Yue-yang Road, Shanghai 200031, China

^d State Key Laboratory for Modification of Chemical Fibers and Polymer Materials, College of Materials Science and Engineering, Donghua University, Shanghai 201620, China

^e Department of Clinical Oncology, Xuhui Central Hospital, 966 Middle Huaihai Road, Shanghai 200031, China

ARTICLE INFO

Article history:

Received 27 August 2013

Accepted 25 September 2013

Available online xxx

Keywords:

Anti-tumor activity
Apoptotic cell death
Bortezomib
Drug delivery
Mesoporous silica
NSCLC

ABSTRACT

Bortezomib (BTZ) is the first clinically approved proteasome inhibitor for treating multiple human malignancies. However, the poor water-solubility and low stability of BTZ and the emergence of tumor resistance have severely restrained its therapeutic efficacy. Herein, we report the application of hollow mesoporous silica nanospheres (HMSNs) in encapsulating BTZ for drug delivery. *In vitro* cell viability assay on human NSCLC H1299 cells, the half-maximum inhibiting concentration (IC₅₀) of HMSNs–BTZ was 42% of that for free BTZ in 48 h treatments. *In vivo* tumor-suppression assay further indicated that HMSNs–BTZ (0.3 mg/kg) showed approximately 1.5 folds stronger anti-tumor activity than free BTZ. Furthermore, we report that more potent induction of cell cycle arrest and apoptotic cell death, along with promoted activation of Caspase 3 and autophagy might mechanistically underlie the improved anti-tumor efficacy of HMSNs–BTZ. Finally, the tumor-suppressing effect of HMSNs–BTZ was enhanced in the presence of wild-type p53 signaling, suggesting a potential enhancement in clinical efficacy with combined p53 gene therapy and BTZ-based chemotherapy. Therefore, the HMSNs-based nanoparticles are emerging as a promising platform to deliver therapeutic agents for beneficial clinical outcomes through lowering doses and frequency of drug administration and reducing potential side effects.

© 2013 Elsevier Ltd. All rights reserved.

1. Introduction

Cancer poses major threat to human health worldwide [1], among which lung cancer is the leading cause of cancer mortality [2,3]. In particular, non-small cell lung cancer (NSCLC) accounts for approximately 80% of all primary lung cancer. Patients with early stage of NSCLC, although deemed suitable for curative treatment, maintain a

significantly high rate of relapse after therapy [4,5]. Patients with advanced cancer are often treated with systemic chemotherapy but response and 5-year survival rate is less than 3% with a median survival of 8–11 months after a standard chemotherapy [6].

Degradation of more than 80% of cellular proteins goes through the ubiquitin–proteasome system (UPS). Proteasome-dependent proteolysis is known to regulate almost all aspects of cellular activity, including cell cycle, apoptosis and intracellular signal transduction [7–9]. Inhibition of the proteasome disrupts protein homeostasis and attenuates multiple signaling pathways that promote tumor transformation has become a very attractive anti-cancer therapy [10–12]. Bortezomib (BTZ), which reversibly binds to the chymotrypsin-like activity of proteasome b5 subunit, PSMB5 [13], was the first proteasome inhibitor clinically approved for treating multiple myeloma [14–17] and mantle cell lymphoma

* Corresponding author. Shanghai Key Laboratory of Molecular Andrology, Institute of Biochemistry and Cell Biology, Shanghai Institutes for Biological Sciences, Chinese Academy of Sciences, 320 Yue-yang Road, Shanghai 200031, China.

** Corresponding author.

E-mail addresses: hu.junqing@dhu.edu.cn (J. Hu), coryhu@sibs.ac.cn, coryhu00@gmail.com (R. Hu).

¹ These authors contributed equally to this work.

[18–20]. Recently, BTZ has been tested on a wide range of human cancer cell lines, but the efficacy varied [21–27]. Particularly, single-agent BTZ in patients with NSCLC has limited activity with responses up to 8% only [28,29]. Meanwhile, clinical complications and high rates of relapse with drug-resistant tumors have also been frequently reported in conventional BTZ chemotherapy [30,31]. BTZ is hydrophobic and dissolves in water with poor solubility (less than 1 mg/ml). Once dissolved in aqueous solution, BTZ is only stable for 8 h at 25 °C [32]. Intravenous administration of hydrophobic agents such as BTZ could cause coagulation in blood capillaries and elicit serious complications, which also lower the effective drug doses [33]. Additionally, the mean elimination time of BTZ is relatively short in patients with advanced malignancies [34]. The inherent low water solubility, low bioavailability and the unstable property of BTZ hinder the clinical use for effective cancer therapy. Hence the development of novel delivery systems for BTZ without the use of organic solvents is indispensable for efficient cancer treatment.

Nanoparticles have been developed for application in cancer therapy as a promising approach to deliver therapeutic agents into targeted organs or cells [35,36]. Among many drug-delivery systems, mesoporous silica nanomaterials is one of the most promising candidates due to their unique properties, including large surface area, highly-hydrophilic nature, easily modifiable surface and pore size, as well as good biocompatibility and chemical inertness [37–42]. Notably, the large surface areas and porous interiors could be used as reservoirs for storing hydrophobic drugs like BTZ. In particular, the hollow mesoporous silica nanospheres (HMSNs), whose highly porous feature of the shell allows the encapsulated drug to easily pass through between the inner void space and surrounding environment, possess even higher drug loading capacity as the interstitial hollow space can selectively and efficiently accommodate more drug molecules [43–46]. Herein, we report rational design and successful development of BTZ encapsulated HMSNs as an effective drug-delivery system (Scheme 1).

2. Materials and methods

2.1. Chemicals and reagents

Cetyltrimethylammonium bromide (CTAB), ammonia aqueous ($\text{NH}_3 \cdot \text{H}_2\text{O}$, 25–28 wt%), and ethanol are analytically pure and were purchased from Sinopharm. 2,2'-Azobis(2-methylpropionamide) dihydrochloride (V-50, >97.0%), [2-(acryloyloxy)ethyl] trimethylammonium chloride (AETAC, 80 wt % in H_2O), Styrene (St, >99.0%, washed through an inhibitor remover column for removing tert-butylcatechol and then distilled under reduced pressure prior to use), Fluorescein isothiocyanate (FITC, 90%), 3-aminopropyl triethoxysilane (APS, 98%), and tetraethylorthosilicate (TEOS, GR) were obtained from Aladdin. Bortezomib (BTZ) was purchased from LC Laboratories. Hoechst 33258 and propidium iodide (PI) were purchased from Sigma. Dulbecco's Modified Eagle Medium (DMEM), fetal bovine serum (FBS), LysoTracker Red DND-99 were obtained from Life Technologies. The following antibodies were used: rabbit anti-Pi-Akt antibody (Signalway Antibody), rabbit anti-Akt antibody (Signalway Antibody), mouse anti-Cyclin B antibody (Santa Cruz), rabbit anti-Caspase 3 antibody (Signalway Antibody), mouse anti-actin antibody (Sigma), rabbit anti-LC 3 antibody (Cell Signaling Technology), WST-8[2-(2-methoxy-4-nitrophenyl)-3-(4-nitro-phenyl)-5-(2,4-disulphophenyl)-2H-tetrazolium (Dojindo).

2.2. Characterization

The morphologies and structures of the products were characterized by a field-emission scanning electron microscope (S-4800)

and a field-emission transmission electron microscope (JEOL, JEM-2100F) at an accelerating voltage of 5 kV and 200 kV, respectively. UV–Vis absorption spectra were measured on UV–Vis 1901 Spectrophotometer (Phoenix).

2.3. Synthesis of hollow mesoporous silica nanospheres

The polystyrene latex with a size ~ 130 nm (PS-130) was prepared through emulsion polymerization [47]. In a typical procedure, 1.0 g of AETAC (80 wt% in H_2O) was dissolved in 390.0 g H_2O in a 500 ml round-bottom flask. 40.0 g styrene was added to the solution and kept stirring at 800 rpm for 30 min. The mixture then was purged with nitrogen for 20 min before heating to 90 °C with an oil bath. Afterwards, 10 ml of an aqueous solution containing 1.0 g V-50 was added. The emulsion was kept at 90 °C for 24 h under nitrogen to allow the polymerization to complete.

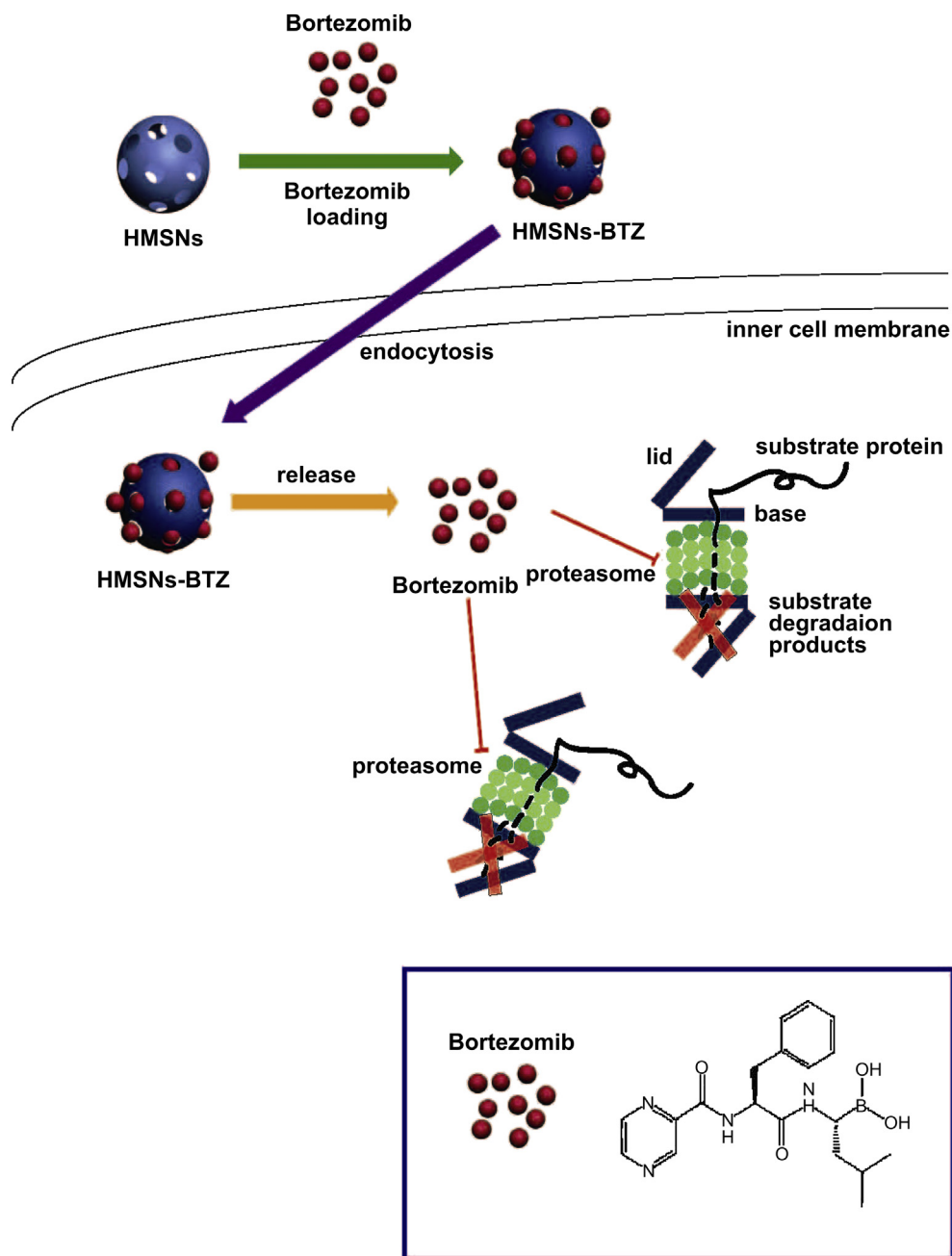
The hollow mesoporous silica nanospheres (HMSNs) with size of ~ 140 nm was prepared as described previously [47]. Typically, 0.80 g of CTAB was dissolved in a mixture of 29.0 g H_2O , 12.0 g ethanol and 1.0 ml $\text{NH}_3 \cdot \text{H}_2\text{O}$. 10.0 g of PS-130 was added dropwise to the above CTAB solution at room temperature under vigorous stirring, followed by sonication for 10 min. The resulted milky mixture was then magnetically stirred for 30 min before dropwise adding of 4.0 g TEOS. The molar ratio of TEOS/CTAB/ethanol/ H_2O / NH_3 was 1.0:0.11:13.0:87.0:0.83, and the TEOS/polystyrene weight ratio was 4.3:1.0. The mixture was kept at room temperature for 48 h before the mesoporous silica coated latex was harvested by centrifugation. The precipitate was washed with ethanol for three times before drying under vacuum at room temperature for overnight. Finally the materials were calcined in air at 800 °C for 8 h with a heating rate at 5 °C/min.

2.4. Preparation of FITC-labeled HMSNs

For modification of the HMSNs' surfaces with amine groups [41,48,49], 40.0 mg of as-prepared HMSNs was dispersed in 15 ml of ethanol by stirring and ultrasonication, then 20 μl of APS and 20 μl of $\text{NH}_3 \cdot \text{H}_2\text{O}$ were added into the above solution, followed by stirring at room temperature for 24 h. Finally, the resultant amine modified HMSNs was separated by centrifugation, washed with ethanol to remove unreacted APS and then dispersed into 10 ml of ethanol, forming amine modified HMSNs/ethanol solution. After that, 10.0 mg (25 μmol) of FITC dispersed in 5 ml of ethanol, and then added into the as-prepared 5 ml of amine modified HMSNs/ethanol solution, followed by stirring at room temperature for 24 h. The resultant was purified by centrifugation and ethanol wash. Notably, the products were protected from light during the sample preparation and storage to prevent photobleaching.

2.5. In vitro bortezomib (BTZ) loading and release

UV–Vis spectroscopy was used to determine the amount of BTZ loaded into the HMSNs [50]. A stock solution of BTZ was used as a standard and serially diluted to concentrations of 6.0–96.0 $\mu\text{g}/\text{ml}$ in PBS. The serial BTZ solutions of different concentrations were measured at 270 nm and a linear fit of the data was created and used as standard curve for the absorption against BTZ concentration. 20.0 mg of as-synthesized HMSNs and 200 μl of BTZ/DMSO solution (10 mM or 3.84 mg/ml) were mixed and stirred at room temperature for 48 h to reach the equilibrium state. The BTZ-loaded HMSNs was collected and washed three times with PBS to remove the unbound BTZ by centrifugation at 14,000 rpm for 10 min and then these supernatant solutions were collected. Encapsulation efficiency was calculated with the following equation: encapsulation efficiency = (weight of BTZ in HMSNs)/(initial weight of BTZ).



Scheme 1. Schematic illustration of the loading and delivery and release of BTZ to the cancer cells by HMSNs.

In the drug release experiment *in vitro*, the hereby prepared BTZ-loaded HMSNs–BTZ were dispersed in 4 ml of PBS and stirred at room temperature. The release solution was centrifuged at an interval of 1 h and the supernatant was collected, then 4 ml of fresh PBS was added to the residual of BTZ-loaded HMSNs complexes. The concentration of BTZ in supernatant was determined by measuring absorbance at 270 nm (A_{270}) and fitting to standard curve.

2.6. Cell culture

Human non-small cell lung cancer (NSCLC) cells (H1299, CRL-5872, HTB-177 cells) were maintained in Dulbecco's modified Eagle's medium and supplemented with 10% fetal bovine serum in a humidified incubator under 5% CO_2 at 37 °C.

2.7. Cellular uptake and internalization

Human non-small cell lung cancer cells H1299 were seeded at a density of 6000 cells/well on 96-well plates (Costar). 100 μL of culture medium containing FITC-labeled HMSNs (50 $\mu\text{g}/\text{ml}$) was added to the culture and incubated for 6 h. The cells were then incubated with Hoechst 33258 (1.0 $\mu\text{g}/\text{ml}$) for another 1 h, then stained with LysoTracker Red DND-99 (100 nM) for 30 min. The cells were washed with phosphate-buffer saline (PBS) three times, and observed on Operetta high content analysis system (PerkinElmer).

2.8. Cell viability assay

Human non-small cell lung cancer (NSCLC) cells (H1299, CRL-5872 or HTB-177) were seeded at a density of 6000 cells/well on

96-well plates. After incubating the cells with PBS (as a control), HMSNs, BTZ, and HMSNs–BTZ of indicated concentrations for 24 h or 48 h, cell viability was assessed in triplicate using WST-8(2-(2-methoxy-4-nitrophenyl)-3-(4-nitrophenyl)-5-(2,4-disulfophenyl)-2H-tetrazolium,monosodium salt) assay with a CCK-8 detection kit (Dojindo Molecular Technologies, Inc., Gaithersburg, MD) according to the manufacturer's instructions. In brief, 10 μ l of CCK-8 solution was added to each well of the plate. The plates were incubated for 4 h and the absorbance measured at 450 nm on a plate reader (Thermo Fisher).

2.9. Cell death fluorescent observation

H1299 cells (6×10^3 cells/well) on 96-well plates were incubated with PBS control, HMSNs (0.5 mg/ml), BTZ (75 nM or 150 nM), or HMSNs–BTZ (containing BTZ 75 nM and 150 nM) for 48 h, then treated with Hoechst 33258 (10 μ g/ml) for another 1 h, stained with propidium iodide (PI, 100 μ g/ml) for 30 min. The cells were washed with PBS three times, and observed on Operetta high content analysis system (PerkinElmer).

2.10. Western blotting

H1299 cells seeded on 6-well plates were incubated with PBS control, HMSNs (0.5 mg/ml), BTZ (150 nM), and HMSNs–BTZ (containing BTZ 150 nM) for 48 h. Then cells were lysed in RIPA buffer (50 mM Tris–HCl, pH 7.2, 150 mM NaCl, 1% NP40, 0.1% SDS, 0.5% DOC, 1 mM PMSF, 25 mM MgCl₂, and supplemented with a phosphatase inhibitor cocktail) and subjected to immunoblotting analysis with indicated antibodies. Actin was probed as internal control.

2.11. Cell cycle and apoptosis analysis

H1299 cells seeded on 6-well plates were treated with PBS control, HMSNs (0.5 mg/ml), BTZ (75 nM and 150 nM) and HMSNs–BTZ (containing BTZ 75 nM and 150 nM) for 48 h. Then the cells were fixed in 70% ethanol at -20°C for 2 h, washed in PBS and stained with propidium iodide (PI, 50 μ g/ml) containing ribonuclease A (50 ng/ μ l) at 37°C for 1 hr, then analyzed with Aria II flow cytometer (BD Biosciences) for sub-G1 peak which indicates the percentage of apoptotic cells in the whole cell population.

2.12. In vivo antitumor effect

Female nude mice (Bi-kai Biotech.) aged 5-week-old were used. H1299 cells (5×10^6 cells) were suspended in Matrigel (BD Biosciences) and injected s.c. into the mice. All animal procedures were performed following protocol approved by the Institutional Animal Care Committee of Shanghai Institute of Biochemistry and Cell Biology. Mice bearing evident tumors were randomly divided into PBS control group, HMSNs group, BTZ group and HMSNs–BTZ group (three mice per group). BTZ, HMSNs and HMSNs–BTZ were dissolved in PBS and directly injected into the tumors at a dose of 0.3 mg/kg (concentration of BTZ) every two days for two weeks. Herein, the HMSNs–BTZ group has an equivalent BTZ dosage to free BTZ group and have an equivalent HMSNs dosage to the HMSNs group. Animals were euthanized with carbon dioxide, tumor masses were isolated and tumor weight measured.

2.13. Statistical analysis

All data are presented as means \pm SEM. The two tailed unpaired Student's *t*-test was used to assess the significance of difference

between two sets of data. Differences were considered to be statistically significant when $P < 0.05$.

3. Results and discussion

3.1. Synthesis and characterization of hollow mesoporous silica nanospheres

The hollow mesoporous silica nanospheres (HMSNs) were prepared using polystyrene latex nanospheres as templates of hollow sphere and surfactant CTAB as pore-generating gas. Then hollow interior was formed after removal of the hard template by calcination, according to a previously published method [45]. From low magnification of scanning electron microscopy (SEM) imaging (Fig. 1A), the as-prepared HMSNs exhibited spherical morphology and possessed a very uniform diameter of ~ 140 nm. These silica nanospheres were nearly transparent to an electron beam during SEM imaging, suggesting the formation of hollow structures, as shown in high magnification of SEM image (Fig. 1B). The low magnification of transmission electron microscopy (TEM) image (Fig. 1C) indicated excellent particle uniformity and the contrast between the dark edge and pale center confirms the formation of hollow sphere. Clearly, from high magnification of TEM image (Fig. 1D), the shell of these HMSNs had a quite rough surface and a mesoporous structure with a thickness of ~ 20 nm.

3.2. In vitro drug release assay

To date, poor water solubility has adversely impacted the clinical applications of many hydrophobic anti-cancer drugs [33,36]. The HMSNs bears many attractive features such as large hollow interior, porous structure, and excellent biocompatibility, which make them particularly suitable for delivery of drugs with low water solubility [46]. Herein, the HMSNs were used as reservoirs for delivering BTZ. The HMSNs were first loaded with BTZ to form BTZ-loaded HMSNs drug-delivery systems by soaking them in a concentrated drug/dimethylsulfoxide (DMSO) solution. The drug-loaded particles were collected by centrifugation. UV–Vis absorption spectroscopy has been used to determine the effective BTZ storage and release. Working standard dilution of BTZ in the range of 6.0–96.0 μ g/ml were measured at 270 nm and a linear fit of the data was created, and used as standard curve for the absorption against BTZ concentration as shown in Fig. 2A. A good linear relationship ($r^2 = 0.999$) was observed for BTZ. Based on UV–Vis absorption measurements, approximately 18.7 μ g of BTZ drug molecules were stored inside 1.0 mg of the HMSNs and an encapsulation efficiency of the BTZ could reach 48.6%. The loading BTZ into HMSNs could probably be attributed to, (1) the physical adsorption of HMSNs derived from large surface area and pore volume [47], and (2) the electrostatic attraction between the negatively charged mesoporous silica surface and ammonia groups of BTZ [37,41,46].

The cumulative drug release profile over a period of 78 h in phosphate-buffer saline (PBS, pH 7.4) at room temperature was shown in Fig. 2B. Cumulative drug release profiles exhibited than 67.7% of drug discharged from HMSNs within 8 h, followed by a sustained and slow release (30.5% of drug released within 70 h). The sustained release properties are favorable for increased drug accumulation in the cancer cells following endocytosis and reduced drug release in normal tissue, thus having a potential to enhance the long-term chemotherapy efficacy and reduce toxic side effect [41].

3.3. Endocytosis of HMSNs

Efficient endocytosis of the nanoparticles is critical for intracellular drug delivery. A fluorescein isothiocyanate (FITC)-labeled

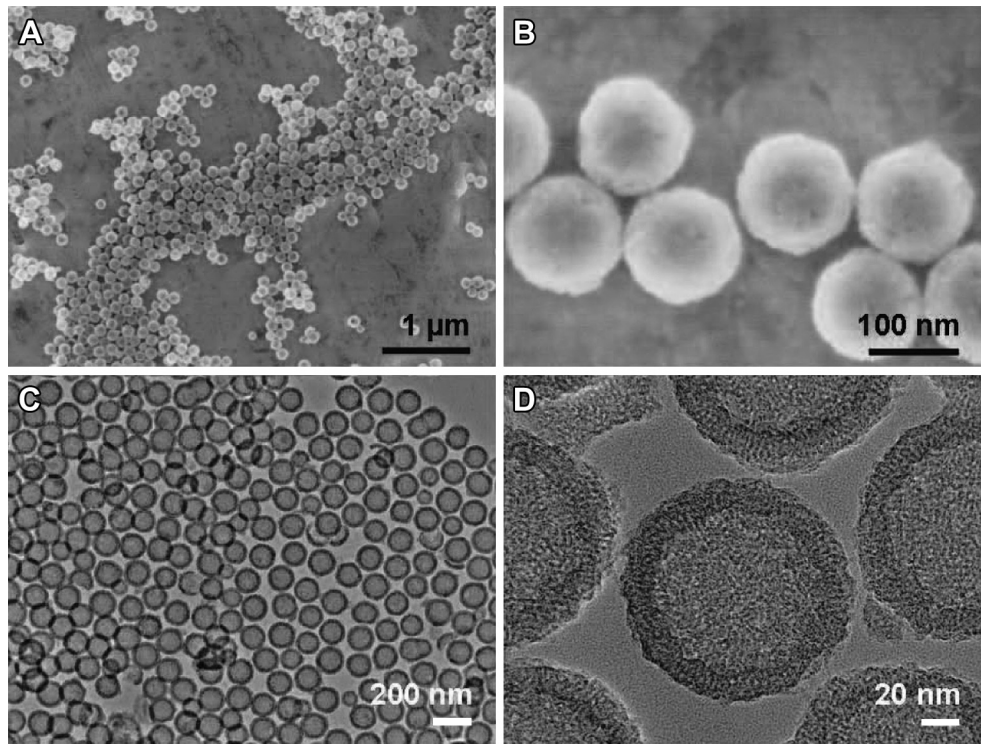


Fig. 1. (A and B) Low- and high-magnifications of SEM images, respectively; (C and D) Low- and high-magnification TEM images, respectively.

HMSNs with high fluorescence was synthesized by modifying the surface of HMSNs with FITC. To confirm the efficient uptake of the nanocarriers by cancer cells, FITC-labeled HMSNs (50 $\mu\text{g}/\text{ml}$) were incubated with H1299 cells for 6 h, then washed with phosphate-buffered saline (PBS) solution to remove the nanoparticles that were not taken up by cells. To determine the intracellular localization of the nanoparticles, cells were stained with Hoechst 33258 (blue) to visualize the nucleus, and LysoTracker Red DND-99 (red) to highlight acidic organelles such as lysosomes and endosomes. The stained live H1299 cells were then subjected to analysis on Operetta high content analysis system (PerkinElmer). As shown in Fig. 3, HMSNs entered cells efficiently after 6 h of incubation. FITC-labeled HMSNs (green) could be observed in numerous cells throughout the entire cell, demonstrating that these nanocarriers can enter the cancer cells with high efficiency. Notably, there were some spots of green fluorescence showing higher fluorescence intensities in some cells, demonstrating the cluster of the HMSNs. In

contrast, some cells exhibited isolated spots of green fluorescence (indicated with white arrows) which overlapped mostly with the red fluorescence of lysosomes and endosomes, suggesting the HMSNs were mainly taken up into the acidic organelles of the cells and then efficiently released to the cytosol, which could eventually disperse throughout the whole cell compartment. This observation demonstrated that the HMSNs, as a membrane-penetrating delivery vehicle for therapeutic molecules (such as drugs, proteins and genes), could enter the cells mainly through endocytosis.

3.4. Cytotoxicity of HMSNs–BTZ on H1299 cancer cells

A high biocompatibility of the drug delivery system is required as a precondition for their applications in cancer treatment. H1299 cells were incubated with HMSNs for 48 h and then cell viability was assessed via WST-8 assay (see “Materials and methods” for details). As shown in Fig. 4A, the HMSNs were not toxic to the cells,

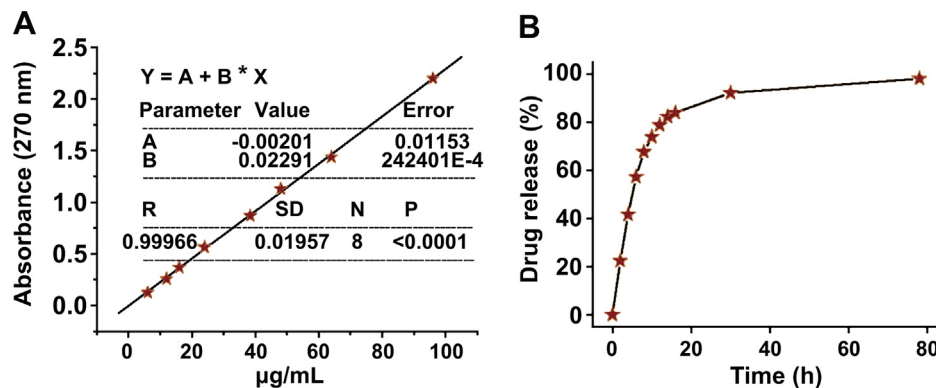


Fig. 2. (A) The standard curve of BTZ by plotting the absorption at 270 nm (A_{270}) against BTZ concentrations. (B) Cumulative profiling of drug release of BTZ from BTZ-loaded HMSNs in phosphate-buffer saline (PBS, pH 7.4) at room temperature.

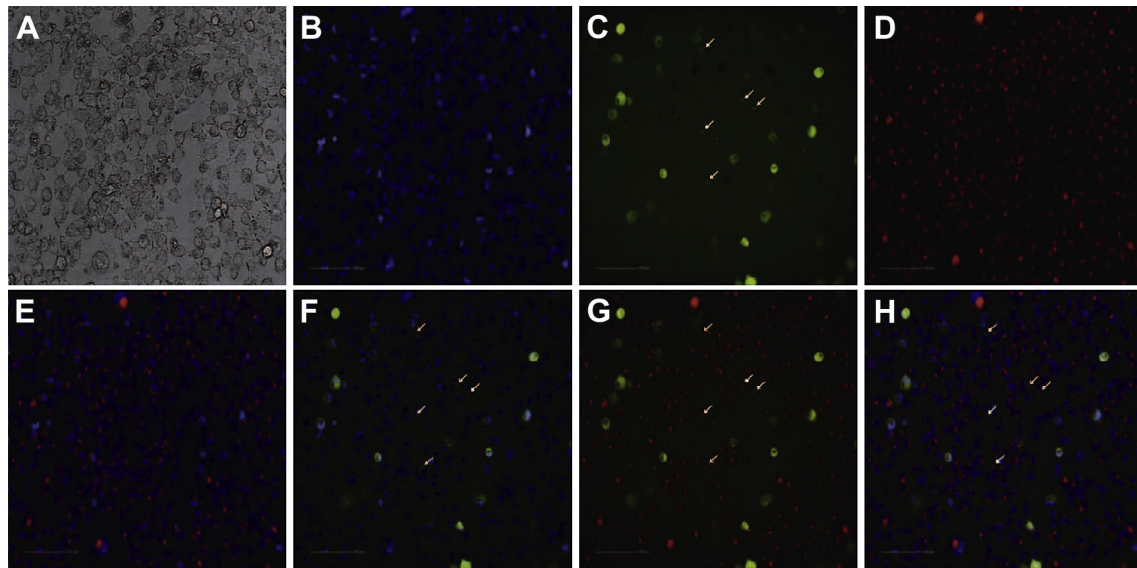


Fig. 3. Uptake and subcellular localization of the FITC-labeled HMSNs in H1299 cells observed by Operetta high content analysis system (PerkinElmer). The cells were incubated with 50 $\mu\text{g}/\text{ml}$ of the FITC-labeled HMSNs for 6 h, then stained with Hoechst 33258 (1 $\mu\text{g}/\text{ml}$) for another 1 h, LysoTracker Red DND-99 (100 nM) for 30 min. (A) Bright field image shows the morphology of corresponding H1299 cells. (B) Blue fluorescence indicates nuclear staining with Hoechst 33258. (C) Green fluorescence indicates the localization of FITC-labeled HMSNs. (D) Red fluorescence indicates the localization of lysosomes stained by LysoTracker Red DND-99. (E) Overlaid image of B and D. (F) Overlaid image of B and C. (G) Overlaid image of C and D. (H) Overlaid image of B, C and D. White arrows in the images indicate complete co-localization of FITC-labeled HMSNs with lysosomes. Scale bar equals 100 μm .

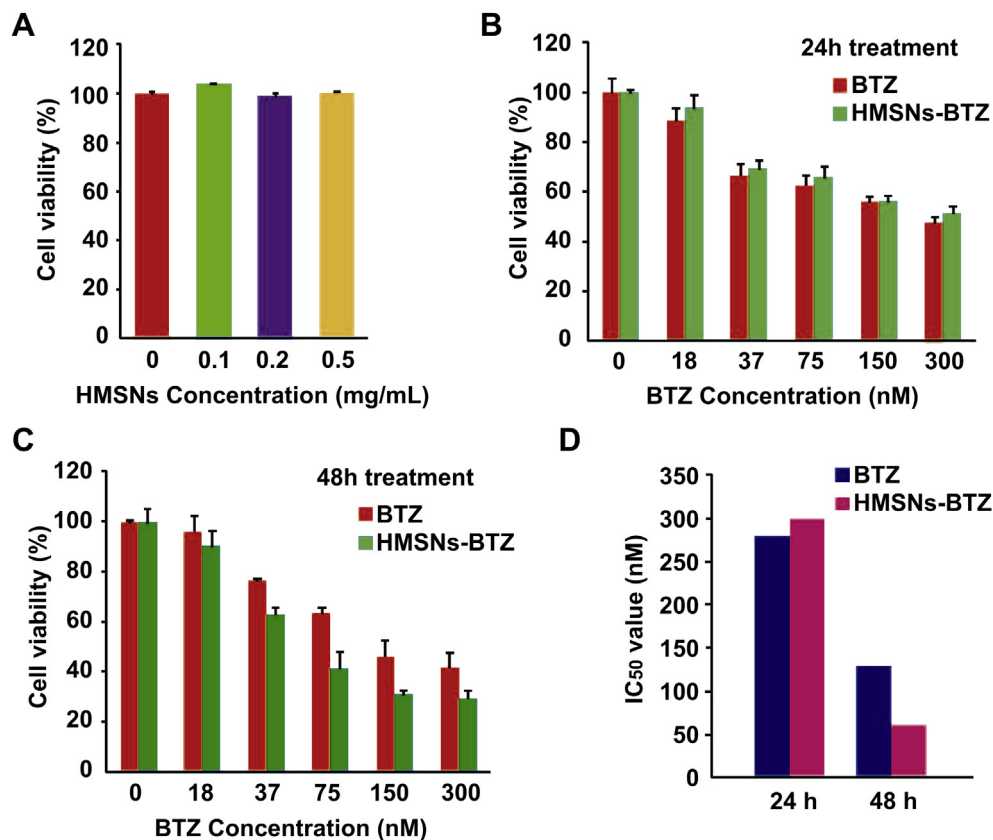


Fig. 4. Cytotoxicity of HMSNs, BTZ or HMSNs-BTZ, on human lung cancer H1299 cells by cell viability assay (WST-8 assay). (A) Viability assay with cells treated with concentrations of HMSNs (0–0.5 mg/ml) for 48 h, BTZ or HMSNs–BTZ (effective concentrations of BTZ, from 0 to 300 nM) on H1299 cells for 24 h (B) or 48 h (C); (D) corresponding IC₅₀ values of BTZ or HMSNs–BTZ for treating H1299 for 24 h or 48 h.

the tested concentration even as high as 0.5 mg/ml, a result indicating excellent biocompatibility of the nanoparticles.

Subsequently, the cytotoxicity comparison of free BTZ and BTZ loaded HMSNs were evaluated. The dose-dependent cytotoxicity on H1299 cancer cells was observed when the cells were treated with either HMSNs–BTZ or free BTZ for 24 h and 48 h, respectively. As shown in Fig. 4B, for the first 24 h treatment, cytotoxicity of free BTZ is comparable to that of HMSNs–BTZ at all concentrations

examined. The half-maximum inhibiting concentrations (IC_{50} value) of free BTZ or HMSNs–BTZ are 280 nM or 300 nM, respectively (Fig. 4D). However, HMSNs–BTZ manifested prolonged cytotoxicity to the cancer cells over a longer period of 48 h drug treatment, and the IC_{50} values of BTZ and HMSNs–BTZ decreased to 130 nM and 55 nM, respectively (Fig. 4C, D).

It is conceivable that the increased and prolonged cytotoxicity of HMSNs–BTZ after cellular uptake might be attributable to the

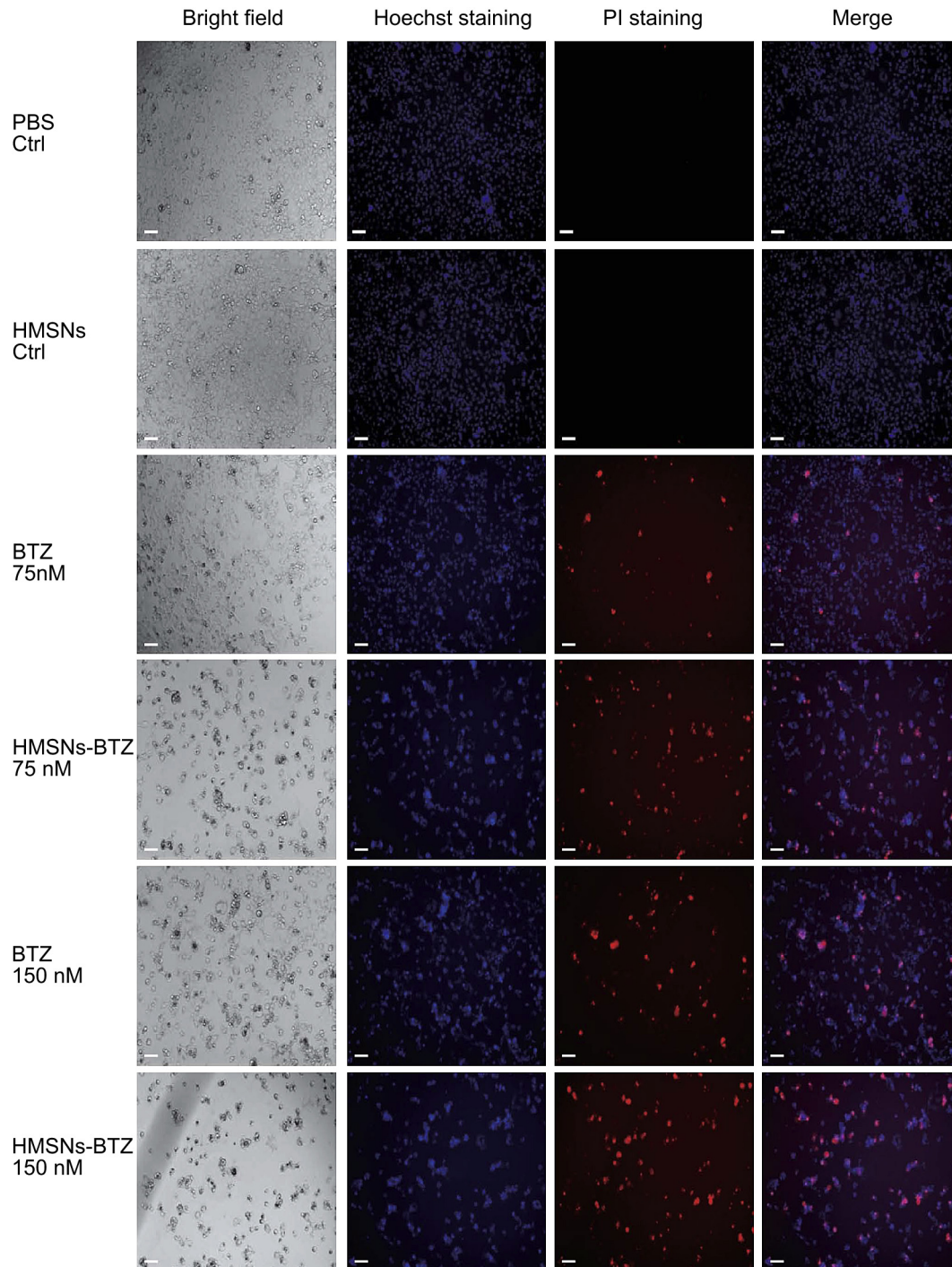


Fig. 5. Comparison of cytotoxicity of BTZ and HMSNs–BTZ to human lung cancer H1299 cells. Cells were treated with PBS, HMSNs (0.5 mg/ml), BTZ (75 nM or 150 nM), or HMSNs–BTZ (of BTZ 75 nM or 150 nM) for 48 h, then stained with Hoechst 33258, Propidium iodide (PI) before observed on Operetta high content analysis system (PerkinElmer). Bright field image shows the morphology of corresponding H1299 cells; cells were stained with Hoechst 33258 to count the total numbers of the cells in each well while PI staining visualizes dead cells. Scale bar equals 100 μ m.

sustained release of the drug molecules from the HMSNs. Therefore, application of HMSNs-based drug delivery system could lead to reduced dose of anticancer drug and decreased frequency of administration in cancer therapy.

To further investigate the mechanism by which HMSNs–BTZ exerted the cytotoxicity, and also to compare the cytotoxicity between HMSNs–BTZ and free BTZ, cell death assay was performed on Operetta high content analysis system (PerkinElmer). The H1299 cells were incubated with PBS control, HMSNs (0.5 mg/ml), BTZ (75 nM and 150 nM), or HMSNs–BTZ (containing BTZ 75 nM or 150 nM) for 48 h, then double stained with Hoechst 33258 (blue,

indicates nucleus) and propidium iodide (PI, red, indicates dead cells). As shown in Fig. 5, the cells treated with a high concentration of HMSNs (50 µg/ml) did not show any abnormality compared to the PBS control, which was consistent with previous data from cell viability assay (Fig. 4A) and further confirmed the biocompatibility of HMSNs. In contrast, chromatin condensation and apoptotic body formation could be readily observed for most of the cells treated with BTZ, as well as HMSNs–BTZ. Moreover, wider distribution and higher fluorescence intensity in propidium iodide (PI) staining, which indicates dead cells of total population, were more prominent in the HMSNs–BTZ group, when compared to that of BTZ

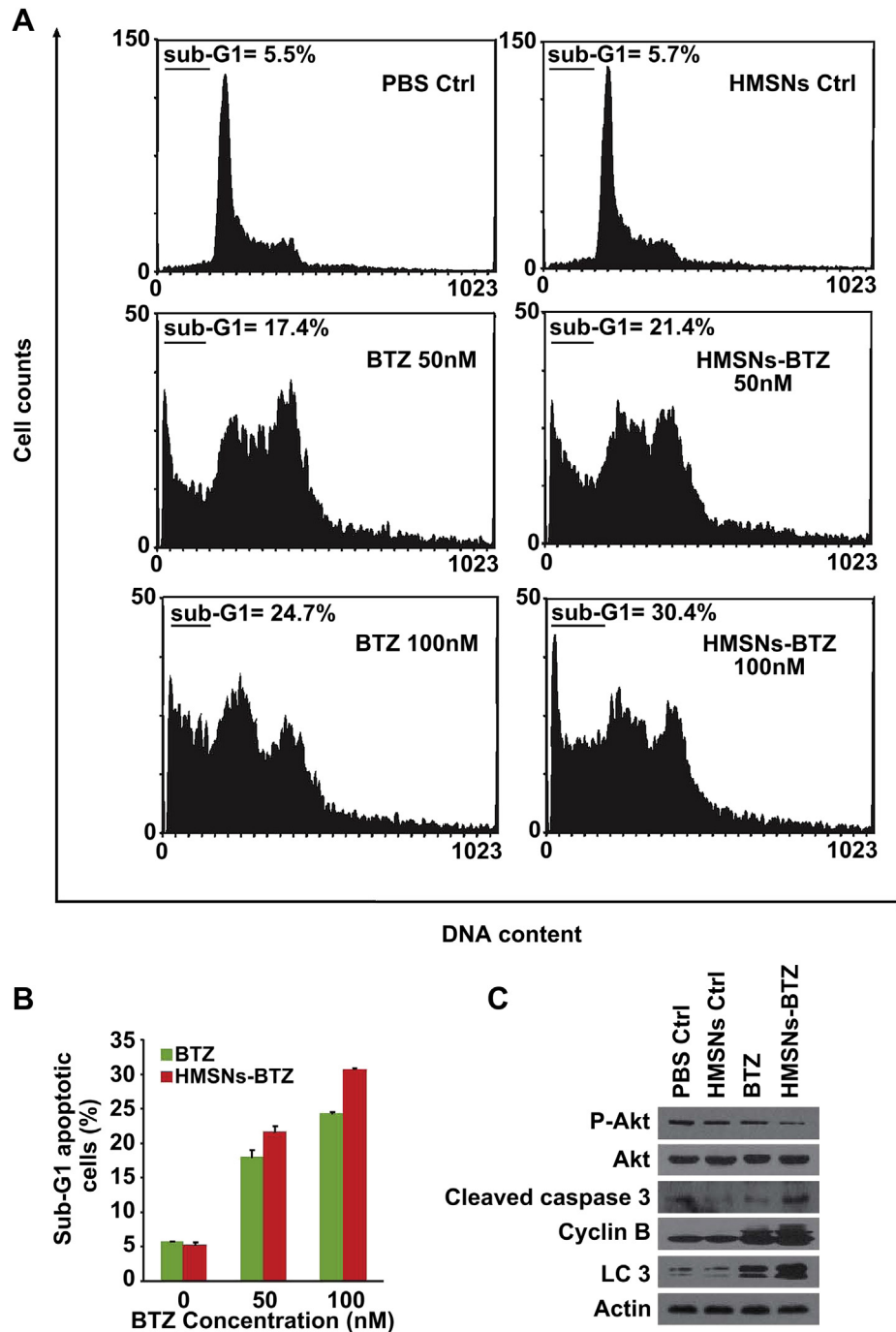


Fig. 6. Flow cytometry analysis to determine the apoptotic sub-G1 cell population in H1299 cells treated with PBS, HMSNs (0.5 mg/ml), BTZ (50 nM or 100 nM), or HMSNs–BTZ (containing BTZ 50 nM or 100 nM) for 48 h (A, B). (C) Effects of BTZ (150 nM) or HMSNs–BTZ (containing BTZ 150 nM) on the endogenous levels of several key regulators in cell cycle or death, probed with indicated antibodies in immunoblotting analysis.

group at the equivalent BTZ concentration, suggesting BTZ-loaded HMSNs might cause more cancer cells to death than that of the free BTZ. Therefore, HMSNs–BTZ might exert higher cytotoxicity to the cancer cells than free BTZ, likely through induction of more apoptotic cell death.

Apoptosis analysis using Flow cytometry analysis has further substantiated this mechanism. H1299 cells were treated with PBS control, HMSNs (0.5 mg/ml), BTZ (75 nM and 150 nM) or HMSNs–BTZ (containing BTZ 75 nM and 150 nM) for 48 h, followed by fixation and propidium iodide (PI, 50 µg/ml) staining. The apoptotic cells, which have a lower DNA content, should fall into those similar to the sub-G1 region in cell cycle on flow cytometry analysis. Therefore, after propidium iodide (PI) staining, the number of cells in the sub-G1 population was quantified to measure the percentage of apoptotic cells. As shown in Fig. 6A, in PBS control group, the percentage of cells in the sub-G1 fraction was low (5.5%), which was in discernible from those treated with HMSNs (5.7%), again indicating the biocompatibility of the nanoparticles. However, significant populations of the cells (17.4%, 24.7%) went into sub-G1 phase when treated with BTZ at 50 nM and 100 nM. Remarkably, the HMSNs–BTZ group scored much more significant increase in the number of cells in the sub-G1 fraction (Fig. 6B). Taken together, the results suggest the stronger tumor-ciding effect of HMSNs–BTZ on H1299 cancer cells might be due to induction of more apoptosis than that by free BTZ at the comparable doses.

Treatment with bortezomib is known to cause cell cycle arrest [51,52] and induce apoptosis in cancer cells [53,54]. It is tempting to ask if HMSNs–BTZ might exert tumor-ciding effect through the same mechanism. H1299 cells were exposed to PBS control, HMSNs (0.5 mg/ml), BTZ (150 nM), or HMSNs–BTZ (containing BTZ 150 nM)

for 48 h. As shown in Fig. 6C, free BTZ indeed stabilized Cyclin B, a key protein in G2/M phase control, presumably through inhibiting its ubiquitylation-proteasome mediate degradation. Remarkably, HMSNs–BTZ caused a stronger accumulation of Cyclin B. On the other hand, Akt, also known as Protein Kinase B (PKB), is a serine/threonine-specific protein kinase that plays a key role in apoptosis, cell proliferation, transcription and cell migration. Under various circumstances, activation of Akt (P-Akt) was shown to overcome cell cycle arrest, we found that P-Akt levels decreased under the BTZ treatment compare to the control, especially in the HMSNs–BTZ group, although the total Akt protein levels kept steady. Meanwhile, we found significant activation of Caspase-3 under HMSNs–BTZ treatment, confirming that apoptotic programs were activated, which was consistent with the results of sub-G1 apoptosis assay in the previous experiments. Interestingly, we also found 48 h treatment with BTZ has resulted in the formation of lipidated ATG8/LC3, an established marker for activation of cellular autophagy [55]. Interestingly, HMSNs–BTZ induces even stronger activation of cellular autophagy.

3.5. Anti-tumor activity of HMSNs–BTZ on H1299 lung tumor xenografts

To further evaluate the tumor-suppressing effect of HMSNs–BTZ *in vivo*, a model for tumorigenicity of H1299 cancer cells in nude mice was established. H1299 cells (5×10^6 cells) were injected s.c. into the female nude mice (aged 5-week-old) with a body weight of approximately 20 g to bear xenografts. After three days, mice bearing visible tumors were randomly divided into PBS control, HMSNs, BTZ or HMSNs–BTZ groups (three mice per group). BTZ,

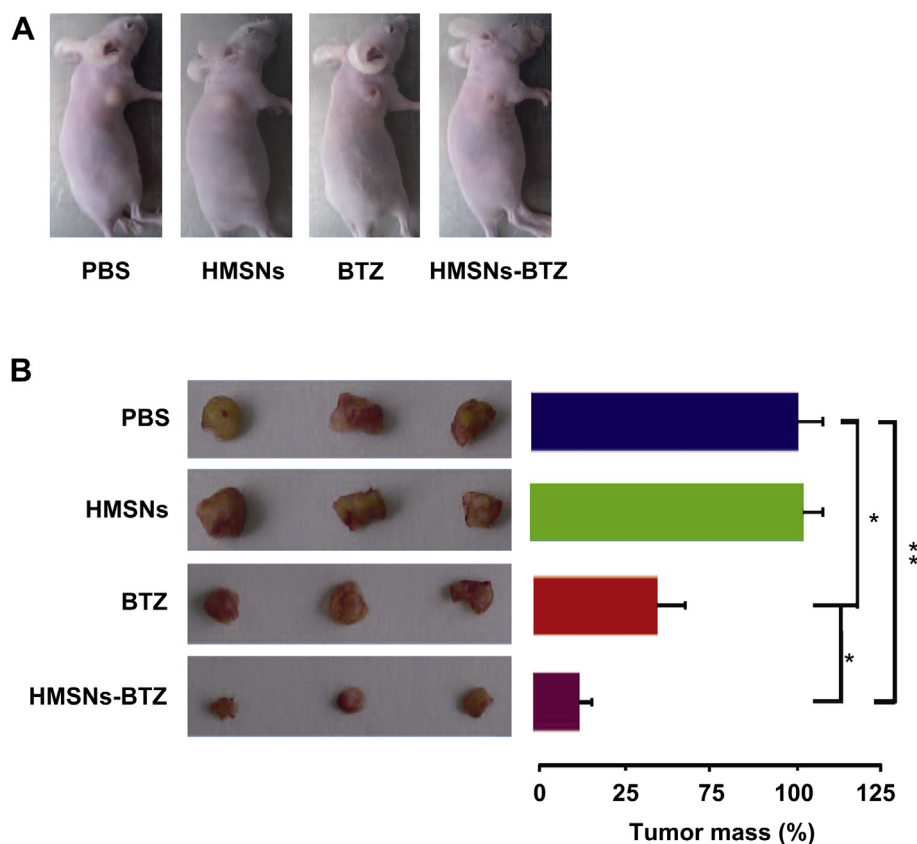


Fig. 7. Anti-tumor effect of HMSNs–BTZ *in vivo*. (A) Representative photos of nude mice bearing tumors formed by H1299 cells after BTZ or HMSNs–BTZ (doses of BTZ at 0.3 mg/kg every two days for two weeks) administration, using those treated with PBS or HMSNs as controls. (B) Weight of the tumor masses dissected from the mice in indicated groups. Data were shown with mean \pm SEM, $n = 3$, * $P < 0.05$, ** $P < 0.01$.

HMSNs and HMSNs–BTZ were dispersed in PBS and directly injected into the tumors at a dose of 0.3 mg/kg (concentration of BTZ) every two days for two weeks. Herein, the HMSNs–BTZ group received BTZ dosage an equivalent to that for free BTZ group. After two weeks, mice were sacrificed and tumors mass dissected and weighed. Images of the tumor in indicated groups along their mean tumor weights are shown in Fig. 7A and B. As anticipated, the tumor sizes of both of the BTZ and HMSNs–BTZ group were smaller than those of the PBS or HMSNs control groups, indicating the tumor inhibitory activity of BTZ. Remarkably, the HMSNs–BTZ group showed much stronger tumor-suppressing effect than that by BTZ only. The average tumor masses in BTZ group were approximately 43% of the control groups, while those of the HMSNs–BTZ group were only 12% of the control groups. This clearly demonstrated that anti-tumor effect of HMSNs–BTZ was over 1.5 fold stronger than BTZ alone. Therefore, in animal models, HMSNs-encapsulation of BTZ also lead to enhanced tumor suppression like it did in cell culture, which consistently highlighted the fact that the improved availability and sustained release BTZ from HMSNs in tumor tissues.

3.6. Efficacy of HMSNs–BTZ on other human NSCLC cells

Somatic mutations in the gene of tumor suppressor p53 are underlying most of human malignancies including non-small cell lung cancer (NSCLC). Up to 50% of all NSCLC contain P53 mutations [56]. Numerous clinical studies pointed that human NSCLC cells with P53 mutations might contribute to poor prognosis and may be relatively more resistant to chemo- or radiation therapy [56,57].

We would like to ask if the tumor-suppressing effects of HMSNs–BTZ would rely on the presence of the functional p53 signaling system in the cancer cells. Therefore, cytotoxic effect of HMSNs–BTZ was further examined on other NSCLC cells including CRL-5872 (P53 mutant) cells and HTB-177 (P53 wild-type) cells, besides H1299 cells. These two lines of cells were then treated with PBS (as a control), HMSNs (0.5 mg/ml), BTZ (100 nM) or HMSNs–BTZ (concentration of BTZ 100 nM) for 48 h, viable cells were examined in triplicates with WST-8 assay. As shown in Fig. 8, HMSNs did not cause visible cytotoxicity on CRL-5872 cells or HTB-177 cells similar to that on H1299 cells (Fig. 4A). As shown in Fig. 8, BTZ treatment induced cytotoxicity in both P53 wild-type and mutant non-small cell NSCLC cells. However, the cytotoxicity efficacy was much stronger on the P53 wild-type HTB-177 cells compared to P53 mutant CRL-5872 cells. Meanwhile, compared to

free BTZ at comparable concentrations, HMSNs–BTZ exerted significantly higher cytotoxicity on both CRL-5872 cells and HTB-177 cells, consistent with previous data observed with H1299 cells (Fig. 4C). Furthermore, the tumor-suppressing effect of HMSNs–BTZ was found to synergize with the presence of wild-type p53 signaling.

Practically, p53 gene therapy has been tested in clinical trials in patients with lung cancer, and several clinical studies have shown a beneficial effect of the combination of P53 gene therapy and chemotherapeutic drugs [58,59]. Our data clearly suggested that more pronounced tumor suppression could be expected if HMSNs–BTZ are administrated in combination with gene therapy using wild-type P53. Given the fact that HMSNs could serve as an excellent vesicle capable of encapsulating and delivering for both small molecule chemicals or macromolecules such as plasmids, co-delivery of tumor suppressor genes such as P53 gene and chemical therapeutic drugs such as BTZ would tremendously impact the clinical treatment of human non-small cell lung cancer.

4. Conclusions

In summary, this study reported the development and primary test of hollow mesoporous silica nanospheres (HMSNs)-based drug delivery of clinically approved proteasome inhibitor BTZ for therapy against human non-small cell lung cancer (NSCLC). The proteasome inhibitor anticancer drug bortezomib (BTZ) loaded nanostructures, which formed HMSNs–BTZ, manifested improved tumor-suppressing effect in both *in vitro* and *in vivo* systems, enhancement of therapy efficacy on NSCLC compare to free BTZ. This might be attributable to the multiple beneficial features of the nanoparticle-based drug delivery system: the improved hydrophilicity, reduced toxicity, excellent dispersibility, sustained drug-releasing property, high stability and excellent biocompatibility. Therefore, HMSNs are emerging as a powerful platform for delivering single or multiple therapeutic agents to treat NSCLC and other human malignancies.

Acknowledgments

This work was supported by funding from National Science Foundation of China to R. H. (31270828, 31070678), and by the grants from the Ministry of Science and Technology, China (2010CB912101, 2012CB910800, 2013CB910900 to R. H. 2011CB915501 to K. R.). R. H. was also supported by Sanofi-aventis SIBS Young Investigator award, and funding from Cancer Center of Xuhui Central Hospital (CCR2012003), Shanghai Institute of Neurosciences, Shanghai Municipal Department of Science and Technology (PJ[2010]00123), Wuzhong Biomedical Center of Suzhou, Jiangshu, Chinese Academy of Sciences. The authors are particularly thankful to Dr. Liang Xue and Ming Chen of Chemical Biology Core Facility of Shanghai Institute of Biochemistry and Cell Biology for their generous guidance of using Operetta high content analysis system (PerkinElmer).

References

- [1] Umar A, Dunn BK, Greenwald P. Future directions in cancer prevention. *Nat Rev Cancer* 2012;12:835–48.
- [2] Perez-Moreno P, Brambilla E, Thomas R, Soria JC. Squamous cell carcinoma of the lung: molecular subtypes and therapeutic opportunities. *Clin Cancer Res* 2012;18:2443–51.
- [3] Houghton AM. Mechanistic links between COPD and lung cancer. *Nat Rev Cancer* 2013;13:233–45.
- [4] Oxnard GR, Binder A, Janne PA. New targetable oncogenes in non-small-cell lung cancer. *J Clin Oncol* 2013;31:1097–104.
- [5] Murray S, Karavasilis V, Bobos M, Razis E, Papadopoulos S, Christodoulou C, et al. Molecular predictors of response to tyrosine kinase inhibitors in patients with non-small-cell lung cancer. *J Exp Clin Cancer Res* 2012;31:77.

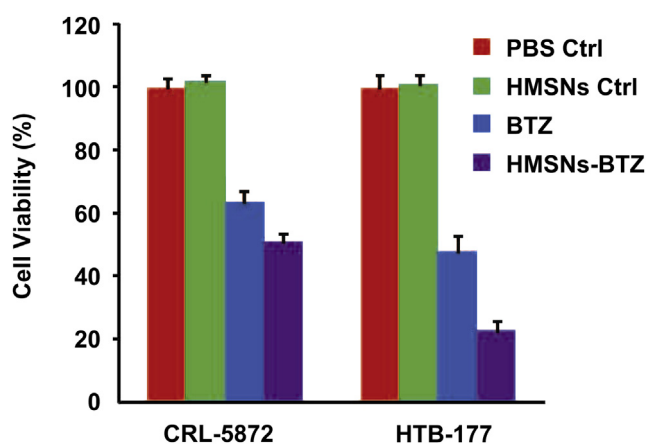


Fig. 8. Evaluation of the cytotoxic effects of HMSNs, BTZ or HMSNs–BTZ on human non-small cell lung cancer (NSCLC) cells (CRL-5872, HTB-177 cells). The cells were treated with PBS, HMSNs (0.5 mg/ml), BTZ (100 nM) and HMSNs–BTZ (equal to 100 nM BTZ) for 48 h, prior to cell viability assay using WST-8. Data were shown with mean \pm SEM, $n = 3$.

- [6] Vilmar AC, Sorensen JB. Customising chemotherapy in advanced nonsmall cell lung cancer: daily practice and perspectives. *Eur Respir Rev* 2011;20:45–52.
- [7] Varshavsky A. Three decades of studies to understand the functions of the ubiquitin family. *Methods Mol Biol* 2012;832:1–11.
- [8] Maupin-Furlow J. Proteasomes and protein conjugation across domains of life. *Nat Rev Microbiol* 2012;10:100–11.
- [9] Pagan J, Seto T, Pagano M, Cittadini A. Role of the ubiquitin proteasome system in the heart. *Circ Res* 2013;112:1046–58.
- [10] Micel LN, Tentler JJ, Smith PG, Eckhardt GS. Role of ubiquitin ligases and the proteasome in oncogenesis: novel targets for anticancer therapies. *J Clin Oncol* 2013;31:1231–8.
- [11] Mullard A. Next-generation proteasome blockers promise safer cancer therapy. *Nat Med* 2012;18:7.
- [12] Wu WK, Cho CH, Lee CW, Wu K, Fan D, Yu J, et al. Proteasome inhibition: a new therapeutic strategy to cancer treatment. *Cancer Lett* 2010;293:15–22.
- [13] Chen D, Frezza M, Schmitt S, Kanwar J, Dou QP. Bortezomib as the first proteasome inhibitor anticancer drug: current status and future perspectives. *Curr Cancer Drug Targets* 2011;11:239–53.
- [14] Richardson PG, Barlogie B, Berenson J, Singhal S, Jagannath S, Irwin D, et al. A phase 2 study of bortezomib in relapsed, refractory myeloma. *N Engl J Med* 2003;348:2609–17.
- [15] Richardson PG, Weller E, Lonial S, Jakubowiak AJ, Jagannath S, Raje NS, et al. Lenalidomide, bortezomib, and dexamethasone combination therapy in patients with newly diagnosed multiple myeloma. *Blood* 2010;116:679–86.
- [16] Kelly KR, Espitia CM, Mahalingam D, Oyajobi BO, Coffey M, Giles FJ, et al. Reovirus therapy stimulates endoplasmic reticular stress, NOXA induction, and augments bortezomib-mediated apoptosis in multiple myeloma. *Oncogene* 2012;31:3023–38.
- [17] Laubach J, Richardson P. Hematology: bortezomib and dexamethasone induction for multiple myeloma. *Nat Rev Clin Oncol* 2011;8:8–10.
- [18] Barr P, Fisher R, Friedberg J. The role of bortezomib in the treatment of lymphoma. *Cancer Invest* 2007;25:766–75.
- [19] Kane RC, Dagher R, Farrell A, Ko CW, Sridhara R, Justice R, et al. Bortezomib for the treatment of mantle cell lymphoma. *Clin Cancer Res* 2007;13:5291–4.
- [20] Koprivnikar JL, Cheson BD. Bortezomib: a proteasome inhibitor with an evolving role in select subtypes of B-cell non-Hodgkin's lymphoma. *Future Oncol* 2012;8:359–71.
- [21] Scagliotti GV, Germonpre P, Bosquee L, Vansteenkiste J, Gervais R, Planchard D, et al. A randomized phase II study of bortezomib and pemetrexed, in combination or alone, in patients with previously treated advanced non-small-cell lung cancer. *Lung Cancer* 2010;68:420–6.
- [22] Lynch TJ, Fenton D, Hirsh V, Bodkin D, Middleman EL, Chiappori A, et al. A randomized phase 2 study of erlotinib alone and in combination with bortezomib in previously treated advanced non-small cell lung cancer. *J Thorac Oncol* 2009;4:1002–9.
- [23] Davies AM, Ho C, Metzger AS, Beckett LA, Christensen S, Tanaka M, et al. Phase I study of two different schedules of bortezomib and pemetrexed in advanced solid tumors with emphasis on non-small cell lung cancer. *J Thorac Oncol* 2007;2:1112–6.
- [24] Voortman J, Checinska A, Giaccone G. The proteasomal and apoptotic phenotype determine bortezomib sensitivity of non-small cell lung cancer cells. *Mol Cancer* 2007;6:73.
- [25] Ceresa C, Giovannetti E, Voortman J, Laan AC, Honeywell R, Giaccone G, et al. Bortezomib induces schedule-dependent modulation of gemcitabine pharmacokinetics and pharmacodynamics in non-small cell lung cancer and blood mononuclear cells. *Mol Cancer Ther* 2009;8:1026–36.
- [26] Nagji AS, Cho SH, Liu Y, Lee JK, Jones DR. Multigene expression-based predictors for sensitivity to vorinostat and velcade in non-small cell lung cancer. *Mol Cancer Ther* 2010;9:2834–43.
- [27] Lilenbaum R, Wang X, Gu L, Kirshner J, Lerro K, Vokes E. Randomized phase II trial of docetaxel plus cetuximab or docetaxel plus bortezomib in patients with advanced non-small-cell lung cancer and a performance status of 2: CALGB 30402. *J Clin Oncol* 2009;27:4487–91.
- [28] Besse B, Planchard D, Veillard AS, Taillade L, Khayat D, Ducourtieux M, et al. Phase 2 study of frontline bortezomib in patients with advanced non-small cell lung cancer. *Lung Cancer* 2012;76:78–83.
- [29] Li T, Ho L, Piperdi B, Elrafei T, Camacho FJ, Rigas JR, et al. Phase II study of the proteasome inhibitor bortezomib (PS-341, Velcade) in chemotherapy-naïve patients with advanced stage non-small cell lung cancer (NSCLC). *Lung Cancer* 2010;68:89–93.
- [30] Song IS, Kim HK, Lee SR, Jeong SH, Kim N, Ko KS, et al. Mitochondrial modulation decreases the bortezomib-resistance in multiple myeloma cells. *Int J Cancer* 2013;133:1357–67.
- [31] Chauhan D, Tian Z, Nicholson B, Kumar KG, Zhou B, Carrasco R, et al. A small molecule inhibitor of ubiquitin-specific protease-7 induces apoptosis in multiple myeloma cells and overcomes bortezomib resistance. *Cancer Cell* 2012;22:345–58.
- [32] Vanderloo JP, Pomplun ML, Vermeulen LC, Kolesar JM. Stability of unused reconstituted bortezomib in original manufacturer vials. *J Oncol Pharm Pract* 2011;17:400–2.
- [33] Wei W, Yue ZG, Qu JB, Yue H, Su ZG, Ma GH. Galactosylated nanocrystallites of insoluble anticancer drug for liver-targeting therapy: an in vitro evaluation. *Nanomedicine* 2010;5:589–96.
- [34] Schwartz R, Davidson T. Pharmacology, pharmacokinetics, and practical applications of bortezomib. *Oncology (Williston Park)* 2004;18:14–21.
- [35] Petros RA, DeSimone JM. Strategies in the design of nanoparticles for therapeutic applications. *Nat Rev Drug Discov* 2010;9:615–27.
- [36] Davis ME, Chen ZG, Shin DM. Nanoparticle therapeutics: an emerging treatment modality for cancer. *Nat Rev Drug Discov* 2008;7:771–82.
- [37] Mamaeva V, Sahlgren C, Linden M. Mesoporous silica nanoparticles in medicine—recent advances. *Adv Drug Deliv Rev* 2013;65:689–702.
- [38] Yang P, Gai S, Lin J. Functionalized mesoporous silica materials for controlled drug delivery. *Chem Soc Rev* 2012;41:3679–98.
- [39] Vivero-Escoto JL, Slowing II, Trewyn BG, Lin VS. Mesoporous silica nanoparticles for intracellular controlled drug delivery. *Small* 2010;6:1952–67.
- [40] Han L, Zhou Y, He T, Song G, Wu F, Jiang F, et al. One-pot morphology-controlled synthesis of various shaped mesoporous silica nanoparticles. *J Mater Sci* 2013;48:5718–26.
- [41] Song G, Li C, Hu J, Zou R, Xu K, Han L, et al. A simple transformation from silica core-shell-shell to yolk-shell nanostructures: a useful platform for effective cell imaging and drug delivery. *J Mater Chem* 2012;22:17011–8.
- [42] Song G, Wang Q, Wang Y, Lv G, Li C, Zou R, et al. A low-toxic multifunctional nanoplatfrom based on Cu₂S₃@mSiO₂ core-shell nanocomposites: combining photothermal- and chemotherapies with infrared thermal imaging for cancer treatment. *Adv Funct Mater* 2013;23:4281–92.
- [43] Conference on the primary prevention of cancer: assessment of risk factors and future directions. *Prev Med* 1980;9:165–332.
- [44] Wang T, Chai F, Fu Q, Zhang L, Liu H, Li L, et al. Uniform hollow mesoporous silica nanocages for drug delivery in vitro and in vivo for liver cancer therapy. *J Mater Chem* 2011;21:5299–306.
- [45] Li L, Tang F, Liu H, Liu T, Hao N, Chen D, et al. In vivo delivery of silica nanorattle encapsulated docetaxel for liver cancer therapy with low toxicity and high efficacy. *ACS Nano* 2010;4:6874–82.
- [46] Wu H, Zhang S, Zhang J, Liu G, Shi J, Zhang L. A hollow-core, magnetic, and mesoporous double-shell nanostructure: in situ decomposition/reduction synthesis, bioimaging, and drug-delivery properties. *Adv Funct Mater* 2011;21:1850–62.
- [47] Qi G, Wang Y, Estevez L, Switzer AK, Duan X, Yang X, et al. Facile and scalable synthesis of monodispersed spherical capsules with a mesoporous shell. *Chem Mater* 2010;22:2693–5.
- [48] Lei J, Wang L, Zhang J. Superbright multifluorescent core-shell mesoporous nanospheres as trackable transport carrier for drug. *ACS Nano* 2011;5:3447–55.
- [49] Liu HM, Wu SH, Lu CW, Yao M, Hsiao JK, Hung Y, et al. Mesoporous silica nanoparticles improve magnetic labeling efficiency in human stem cells. *Small* 2008;4:619–26.
- [50] Sekhar CK, Sudhakar P, Reddy GR, Babu PV, Swamy NL. A new UV-method for determination of bortezomib in bulk and pharmaceutical dosage form. *Int J Pharm Bio Sci* 2013;3:623–7.
- [51] Hong YS, Hong SW, Kim SM, Jin DH, Shin JS, Yoon DH, et al. Bortezomib induces G2-M arrest in human colon cancer cells through ROS-inducible phosphorylation of ATM-CHEK1. *Int J Oncol* 2012;41:76–82.
- [52] Tamura D, Arai T, Tanaka K, Kaneda H, Matsumoto K, Kudo K, et al. Bortezomib potentially inhibits cellular growth of vascular endothelial cells through suppression of G2/M transition. *Cancer Sci* 2010;101:1403–8.
- [53] Yang F, Jove V, Chang S, Hedvat M, Liu L, Buettner R, et al. Bortezomib induces apoptosis and growth suppression in human medulloblastoma cells, associated with inhibition of AKT and NF-κB signaling, and synergizes with an ERK inhibitor. *Cancer Biol Ther* 2012;13:349–57.
- [54] Lioni M, Noma K, Snyder A, Klein-Szanto A, Diehl JA, Rustgi AK, et al. Bortezomib induces apoptosis in esophageal squamous cell carcinoma cells through activation of the p38 mitogen-activated protein kinase pathway. *Mol Cancer Ther* 2008;7:2866–75.
- [55] Klionsky DJ, Abeliovich H, Agostinis P, Agrawal DK, Aliev G, Askew DS, et al. Guidelines for the use and interpretation of assays for monitoring autophagy in higher eukaryotes. *Autophagy* 2008;4:151–75.
- [56] Huang CL, Yokomise H, Miyatake A. Clinical significance of the p53 pathway and associated gene therapy in non-small cell lung cancers. *Future Oncol* 2007;3:83–93.
- [57] Neukirchen J, Meier A, Rohrbeck A, Garcia-Pardillos G, Steidl U, Fenk R, et al. The proteasome inhibitor bortezomib acts differently in combination with p53 gene transfer or cytotoxic chemotherapy on NSCLC cells. *Cancer Gene Ther* 2007;14:431–9.
- [58] Jiang T, Zhou C, Gu J, Liu Y, Zhao L, Li W, et al. Enhanced therapeutic effect of cisplatin on the prostate cancer in tumor-bearing mice by transfecting the attenuated salmonella carrying a plasmid co-expressing p53 gene and mdm2 siRNA. *Cancer Lett* 2013;337:133–42.
- [59] Xu Q, Leong J, Chua QY, Chi YT, Chow PK, Pack DW, et al. Combined modality doxorubicin-based chemotherapy and chitosan-mediated p53 gene therapy using double-walled microspheres for treatment of human hepatocellular carcinoma. *Biomaterials* 2013;34:5149–62.